Automated Network Analyzers for the 0.9- to 12.4-GHz Range

By J. G. EVANS, F. W. KERFOOT, and R. L. NICHOLS

Two highly accurate automated network analyzers have been developed to cover the frequency ranges of 0.9 to 4.2 GHz and 3.7 to 12.4 GHz. In addition to the directly measured quantities of insertion loss and phase, the analyzers provide insertion delay, impedance, and two-port parameters as derived quantities.

The functional architecture of the systems is described along with some of the novel techniques used to obtain the high signal-to-noise ratios and system stabilities needed for the precise measurements of loss, phase, and delay. General descriptions of these techniques are given along with some of the design considerations.

Experimental results that demonstrate measurement accuracy are presented for one-port and two-port devices using both coaxial and waveguide connectors.

I. INTRODUCTION

New automated measuring instrumentation has been developed for making network and component characterizations in the microwave frequency range from 0.9 to 12.4 GHz. The development was stimulated by characterization requirements growing out of the design of new communication systems and the redesign of older systems. These systems are achieving greater capacity due to advances in technology, both in the areas of improved analysis and improved components. These advances have led to requirements on measurements at micro-

wave frequencies that heretofore had been needed only at lower frequencies.

This new instrumentation was implemented as an extension to the Computer Operated Transmission Measuring Sets (COTMS)[1] operating in the Transmission Technology Laboratories at Bell Laboratories. This implementation avoids the duplication of costly common equipment and allows the utilization of many of the proven COTMS measurement techniques.

The microwave instrumentation, in concert with the COTMS system, is intended for the characterization of linear two-port networks, either active or passive. Measurement terminals are provided for networks with either coaxial or waveguide terminals. Provision is made for complete four-parameter characterization of network elements such as transistors (e.g., H parameters, Y parameters).

The full 0.9- to 12.4-GHz frequency range is covered by two microwave systems of very similar design. The lower frequency system, completed in November 1972, covers the range 0.9 to 4.2 GHz.* Its first applications were in characterizing solid state components. The second instrument, completed in May 1971, covers the range 3.7 to 12.4 GHz,† spanning the most widely used common-carrier frequency bands. It found immediate use in characterizing filter elements, and later complete networks for the TN1 radio system.

This paper reviews the measurement capabilities and the overall design of both measuring systems. Several system-design considerations of special interest and error mechanisms that limit accuracy are described. This paper concludes by presenting experimental results that illustrate the applications of the measurement systems and demonstrate their high measurement accuracy.

II. MEASUREMENT SET CHARACTERISTICS

2.1 General

The two microwave measuring sets which cover the frequency ranges of 0.9 to 4.2 GHz and 3.7 to 12.4 GHz are fully automated network analyzers that were specifically designed for high-accuracy measurements. The sets are extensions of the 50-Hz to 1-GHz Computer Operated Transmission Measuring Set (COTMS). The COTMS system provides input frequencies for the microwave signal source, IF detection circuitry, and the control computer. Extensive use is made of the computation capability to enhance measurement convenience and accuracy. Measurements are made under computer direction and the

---

* For brevity this system will be referred to as the 1- to 4-GHz measuring set.
† For brevity this system will be referred to as the 4- to 12-GHz measuring set.

calculations for derived parameters are made in real time. Accuracy is enhanced by the correction of known systematic errors and the averaging of random errors. The resulting measurement speed and accuracy are significantly greater than those previously achieved with manual techniques.

2.2 Measurements

The basic quantities measured by the test sets are loss (or gain) and phase. Insertion loss and insertion phase of a network are determined by subtracting the loss and phase obtained with the test set connectors directly connected from the loss and phase measured with the network inserted between the connectors. Special care was taken to achieve an uncertainty in test-port impedance of less than 2 percent on both the coaxial and waveguide test ports in order to minimize impedance mismatch errors.

Envelope delay, τ, is a derived parameter approximated from insertion-phase measurements at two closely spaced frequencies.

$$\tau = \frac{\partial \theta}{360 \partial F} \doteq \frac{\theta_2 - \theta_1}{360(F_2 - F_1)} \text{ for } \theta \text{ in degrees.} \tag{1}$$

The return loss or reflection coefficient of a single-port device under test (DUT) is also a derived parameter.[2] The measurement is made with the hardware switched (for example, see the S_{11} and S_{22} configurations in Fig. 4) to couplers on the coaxial test ports and magic tee hybrids on the waveguide test ports. Three measurements with independent reflection calibration standards are used to substantially reduce errors associated with impedance mismatches and poor coupler directivity.[2]

The four-parameter characterization of a DUT entails a complicated set of calibration measurements and switching of the hardware into four independent measurement configurations. The four measurements are closely related to the scattering (S) parameters[2] and are easily transformed to other parameter representations. Determination of the S parameters entails the measurement of three reflection coefficient standards on each test port and a transmission standard connecting the test ports. Automatic switching provides the proper interconnections for two transmission and two reflection measurements corresponding to $S21$, $S12$, $S11$, and $S22$. The measurements are followed by a calculation to convert S parameters that are referenced to test set impedances to S parameters referenced entirely to the calibration standards, thereby eliminating any impedance-mismatch errors associated with imperfect test set impedances.[3] More details on the hardware used for the above measurements are presented in later sections.

2.3 Test set performance

The uncertainties of measurements made on both test sets are dependent upon random errors, uncorrected systematic test set errors, and uncertainties in the calibration standards. The random errors can be reduced by signal averaging. For a typical measurement, the user can specify an upper bound on the numerically computed variance of the mean of every directly measured quantity. Averaging slows down the measurement rate. The measurement rate is five frequency points per second taking a single observation. The rate decreases to one frequency point per second if 32 observations are averaged. The typical standard deviation of a single observation at low insertion loss is 0.0017 dB and 0.01 degree.

Table I gives a representative list of the quantities measured and their respective resolutions. The resolution, or differential accuracy, is important in the characterizations of the small loss and phase variations in the passband of a filter.

Systematic test set errors may give rise to uncertainties in absolute characterizations that are larger than the differential uncertainties. Some of these errors, such as detection nonlinearity, are functions of many parameters and are not practical to remove by computation.

Table I — Test set performance

Characteristic	Range	Resolution
Frequency	0.9 to 4.2 GHz; 3.7 to 12.4 GHz in two test sets.	1 Hz
Test rate	Five measurements per second with no averaging for insertion loss and phase	
Insertion measurements*		
Loss	0 to 80 dB	0.002 dB
Phase	0° to 360°	0.01°
Delay	$(0 \text{ to } 1980)/\Delta F$ ns†	$0.06/\Delta F$ ns
Reflection measurements*		
Reflection coefficient	0 to 1	0.02%
Two-port measurements*		
Reflection		
parameters ($S11$, $S22$)	0 to 1	0.02%
Transmission		
parameters ($S12$, $S21$)	0 to 80 dB	0.002 dB
	0° to 360°	0.02°
Incident power level	−15 to −55 dBm (0.9 to 4.2 GHz)	1.0 dB
	−5 to −30 dBm (3.7 to 12.4 GHz)	2.0 dB

* Loss and phase random uncertainties increase as loss increases, decreasing the signal-to-noise ratio. The variance of a single measurement increases as follows:

$$\sigma_{\text{loss}} = 0.0017 \times 10^{L/20} \text{ dB}$$
$$\sigma_{\text{phase}} = 0.01 \times 10^{L/20} \text{ deg.}$$

L is the loss in dB of the DUT. The random uncertainty can be reduced by averaging.

† ΔF is the frequency difference in eq. (1) expressed in MHz.

They have been reduced by careful system design to a magnitude typically less than the relationships given below when the best available calibration standards are used.[*]

$$|\Delta Sjj| \leq 0.0015(1 + F/12)|1 - Sjj^2 - Sij \cdot Sji| \qquad (2)$$

$$\left|\frac{\Delta Sij}{Sij}\right| \leq 0.0001(1 + F) + 0.0001|Sij|^{-1}$$
$$+ K(1 + F/12)(|S11| + |S22|) \qquad (3)$$

$K = 0.01$ for a simple insertion measurement

$K = 0.002$ for mismatch errors after computer correction.

The parameter (F) is the measurement frequency expressed in gigahertz. The family of parameters (Sij) are the scattering parameters of the device under test.

Equation (2) can be applied to a one-port reflection coefficient characterization by setting $|S12 \cdot S21|$ equal to zero. Uncertainty in the characterization of the standards is the dominant contributor to this partially empirical relationship.

Equation (3) is composed of a crosstalk uncertainty, an impedance mismatch uncertainty, and a residual uncertainty from many other mechanisms. When a simple insertion measurement is made without compensation for the deviation of the test set impedances from nominal values, then the coefficient on the last term must be increased from 0.002 to 0.01. A more comprehensive discussion of the error mechanisms is given in Section V.

III. BLOCK DIAGRAM DESCRIPTION

3.1 Overall description

A simplified block diagram illustrating the relationship between COTMS and the broadband microwave test sets is shown in Fig. 1. The test sets are quite similar in system design. They consist of source, comparison unit, heterodyne converter, and interface circuitry.

The COTMS source supplies a computer-controlled low-frequency input signal to source circuitry in each test set. The microwave measurement frequency is developed in the source circuitry by heterodyning and frequency multiplication of the input signal. Signal purity of the output signal is enhanced by computer-controlled YIG filters.

The comparison circuitry interconnects the source and detector via a switching network that rapidly interchanges an unknown path, containing the DUT, and a standard path. Full two-port characteri-

---

[*] Equation (2) is valid if the uncertainty in the reflection coefficients of the impedance standards is less than 0.001. Equation (3) is valid if the uncertainty in $S12$ and $S21$ of the transmission standard is less than 0.0001.

zation of the unknown is provided by additional switching circuitry in the unknown path.

The heterodyne circuit provides a fixed intermediate frequency input signal to the computer-controlled COTMS detector. This signal contains information on the differences in amplitude and phase between the unknown and standard paths. The heterodyne circuit also provides a phase-reference input signal to the COTMS detector at the same fixed intermediate frequency.

The interface provides digital control of the test system circuitry by the COTMS computer and informs the computer of circuit status. All digital lines between COTMS and the test systems pass through the interface. Manual control of each line is also provided by a toggle switch for maintenance and other special purposes.

3.2 Source

The test frequency in each applique is developed by heterodyning a signal at frequency f_1 received from COTMS with a signal at frequency f_2 (see Fig. 2). The signal f_2 is derived from reference signals coherent with the synthesizer-derived signal f_1. The signal at frequency $f_1 + f_2$ is applied to the input of a comb generator which produces a harmonic
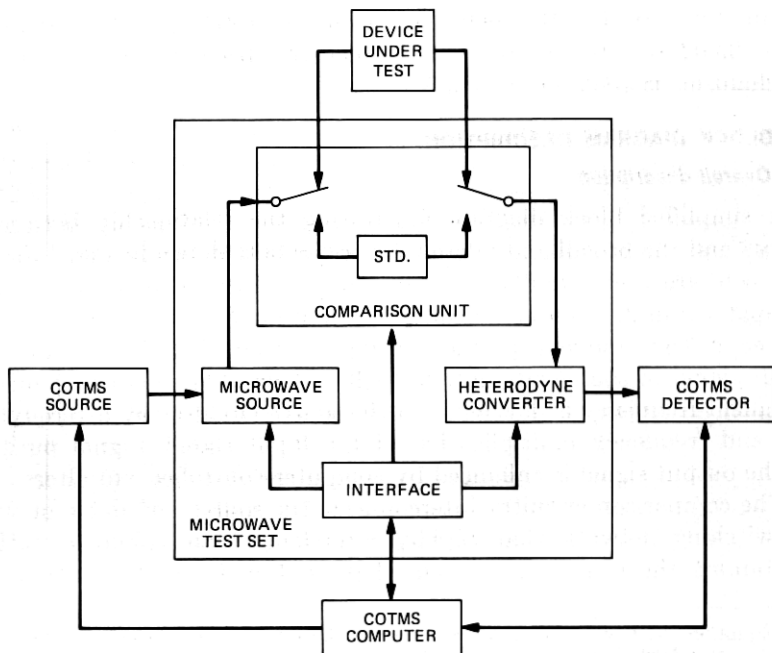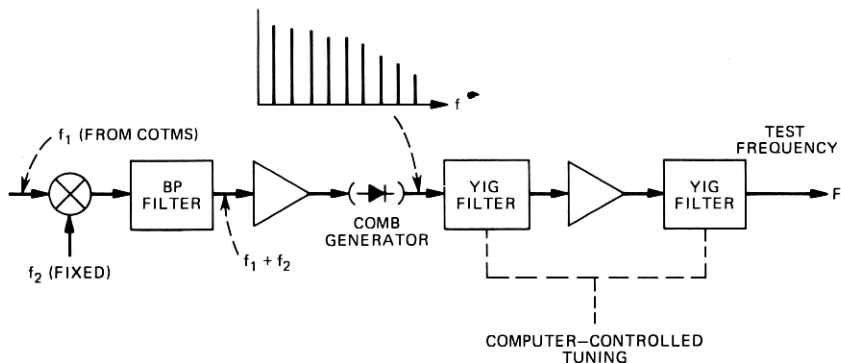

Fig. 1—Simplified block diagram of the COTMS-microwave measuring systems.

Fig. 2—Block diagram of the source circuitry.

1–4 GHz MEASURING SET : f_2 = 198 MHz, 22 MHz $\leqslant f_1 \leqslant$ 77 MHz

4–12 GHz MEASURING SET : f_2 = 825 MHz, 75 MHz $\leqslant f_1 \leqslant$ 300 MHz

output spectrum extending beyond 13 GHz. A single sinusoidal harmonic is selected by four stages of computer-controlled YIG filtering, producing a test signal at frequency $F = N(f_1 + f_2)$. This weak signal is amplified with solid state amplifiers in the 1- to 4-GHz test set and with a traveling-wave-tube amplifier in the 4- to 12-GHz test set.

3.3 Heterodyne section

In the heterodyne section (see Fig. 3), the microwave source signal (F) is split to excite the DUT, generate a reference-phase signal, and generate the local-oscillator signal. The local-oscillator (LO) signal and the signals at frequency F are combined to form fixed intermediate-frequency signals (IF) which are sent to the COTMS detection circuitry. These IF signals are processed by COTMS to extract phase and amplitude information.

The source signal applied to the upper path shown in Fig. 3 excites the DUT in the comparison circuit. The DUT modulates the amplitude and phase of this signal, which are ultimately detected in COTMS. To be compatible with the COTMS frequency range, it is necessary to heterodyne this signal with an LO signal to generate a lower-frequency IF signal.

A reference signal is necessary to make a phase measurement. This reference signal is generated in the lower path in Fig. 3 in an almost identical fashion as that described above.

The LO signal common to both IF mixers is offset from the measurement frequency by 0.495 GHz. This signal is generated by the mixer
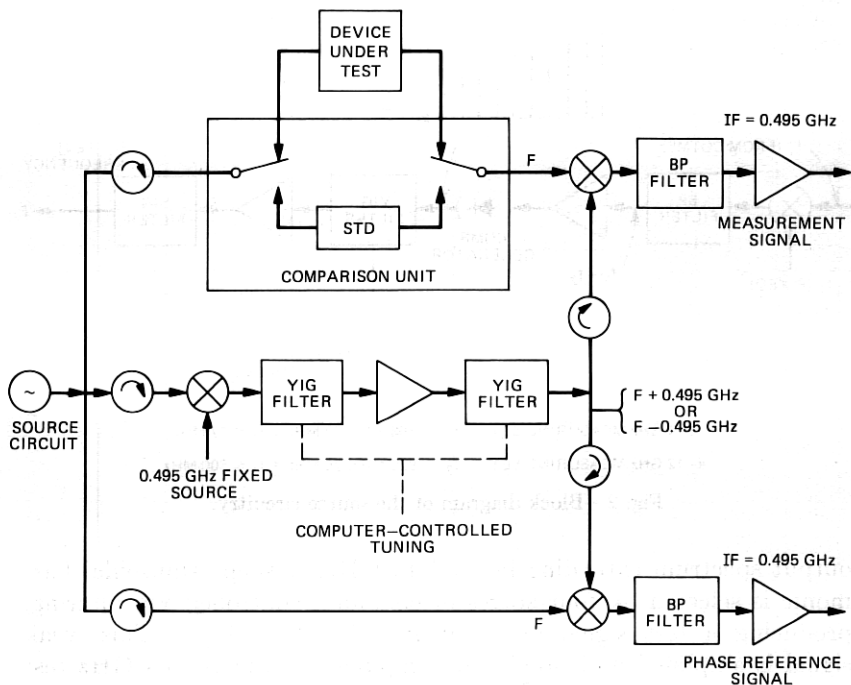
Fig. 3—Block diagram of the heterodyne circuitry.

circuit shown in the middle path of Fig. 3. The fixed 0.495-GHz signal is derived from reference signals coherent with the synthesizer-based test signal F. The overall LO path bandwidth is minimized by switching from the $F + 0.495$ GHz sideband to the $F - 0.495$ GHz sideband at each test set's midband point. The proper sideband is selected by four stages of YIG filtering. This filtering attenuates all unwanted tones, especially the F tone, by 140 dB with respect to the wanted sideband tone. This technique for the generation of the LO signal eliminates the need for a second microwave source and achieves a coherence between the F and the $F \pm 0.495$-GHz signals that is important in reducing phase noise. This latter consideration is discussed further in Section 4.4.

3.4 Comparison circuit

The comparison circuit is a switching network which excites the DUT at various test ports and performs a rapid comparison switching to an internal transfer standard. In each test set, there are test ports with a reflection purity exceeding 40 dB used for insertion measurements and a four-configuration switching network for the measurement

of the four S-parameters of a two-port device. This latter network is illustrated in Fig. 4. A computer-directed calibration procedure provides the data for the automatic removal of errors arising from cross-talk and impedance deviations. Additional test ports are provided in the 4- to 12-GHz applique for the measurement of reflection coefficients in three waveguide sizes.

The rapid comparison switch allows measurements in a differential mode to increase accuracy. The DUT is compared to the internal standard and the difference in loss $(Mx - Ms|\mathrm{dB})$ and phase $(\theta_x - \theta_s)$ are recorded. Similarly, an external standard is measured, obtaining $(Mz - Ms)$ and $(\theta_z - \theta_s)$. The loss and phase of the DUT relative to the external standard are derived from the simple operations:

$$(Mx - Mz) = (Mx - Ms) - (Mz - Ms) \text{ dB} \qquad (4)$$

$$(\theta x - \theta z) = (\theta x - \theta s) - (\theta z - \theta s) \text{ deg.} \qquad (5)$$

This technique eliminates errors from drifts in the hardware external to the comparison switches and from the effects of asymmetry in the two switch positions. The comparison rate was chosen as 30 Hz to achieve an effective filtering of 60 Hz AC interference.

3.5 Interface circuitry

Digital control of the test sets by the COTMS computer and computer monitoring of their circuit status is provided by the interface circuitry.
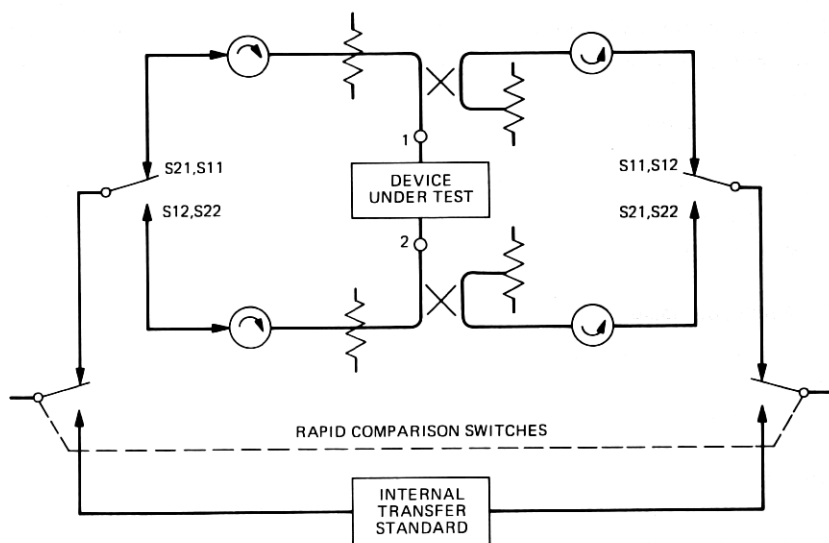

Fig. 4—Block diagram of the comparison circuit.

This circuitry processes all digital lines between the sets and COTMS, with manual control of each line also provided by a toggle switch. Computer or COTMS-generated logic signals provide control of the following major functions: s–x comparison switching, test-port configuration selection, DUT RF level control, and YIG filter tuning through a D/A converter.

The interface also monitors critical test system circuits for operation within established limits. Detection of an out-of-limit or fault condition halts the measurement process and energizes a panel lamp indicating the condition. Interface panel meters associated with each of the monitored circuits are also provided as troubleshooting aids.

IV. SYSTEM DESIGN CONSIDERATIONS

4.1 General

Previously, measurements of the required accuracy (see Table I) were made only with equipment of limited range and with painstaking care on a point-by-point basis. The need for measurements over extended ranges, with measurements performed rapidly and automatically, required some special system designs. Some of the techniques needed to achieve frequency accuracy, high signal-to-noise ratios, thermal stability, and impedance purity are discussed below.

4.2 Frequency accuracy

Frequency accuracy is necessary to minimize the uncertainties in the measurement of loss, phase, and delay of networks that have large variations of these parameters with frequency. The delay determination (see eq. 1) is directly sensitive to inaccuracies in frequency which lead to uncertainties in the quantity $(F_2 - F_1)$.

Exceptional frequency accuracy is achieved in each test system by the generation of all signals from the synthesizer and reference signals from COTMS; these signals are derived from the same high-quality crystal source.

4.3 Amplitude noise

An amplitude signal-to-noise ratio exceeding 80 dB was a design objective to achieve a loss-measurement resolution of 0.002 dB for small values of loss. This was achieved through the use of a narrow detection bandwidth in COTMS (500 Hz) and through noise-suppression circuitry.

The amplitude-noise suppression occurs in the level-control circuitry which appears in the source and local-oscillator sections. These level circuits serve the dual function of maintaining nominal signal
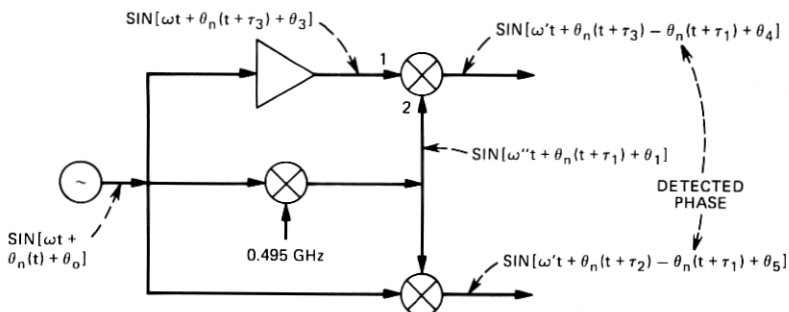
Fig. 5—Phase-noise cancellation mechanism.

levels and suppressing amplitude noise in a bandwidth exceeding 500 Hz centered about the leveled carrier signals.

4.4 Phase noise

A design consideration of considerable importance was the ability to measure delay with small uncertainty. The objective was to have an uncertainty not exceeding 0.1 ns (rms) when measuring narrow filters, where the frequency aperture, $F_2 - F_1$ in eq. (1), couldn't exceed 0.5 MHz. This objective is commensurate with a signal-to-phase noise ratio exceeding 80 dB.[*]

Phase noise was reduced to accomplish this objective in two ways: the first by reducing the phase noise present on the microwave signal and the second by noise cancellation in the frequency-conversion and phase-detection circuitry. Phase noise is increased in the microwave source generation process, for it is multiplied in direct proportion to frequency multiplication. The amount of multiplication has been reduced in each measuring system by the use of an intermediate stage of heterodyne conversion with a relatively phase-noise-free signal f_2 (see Fig. 2). The reduction is approximately four times or 12 dB. At 12 GHz, where the multiplier is largest, the phase signal-to-noise ratio is approximately 30 dB.

The second means of phase-noise reduction is by cancellation, of which there are two mechanisms. The first is demonstrated in Fig. 5.

Phase noise in the source $\theta_n(t)$ propagates via the measurement path and the LO generation path, appearing at ports 1 and 2 of the measurement-path IF mixer. The phase terms $[\theta_i; i = 0, 1, 2, \cdots, 5]$ are constants that are not important to this evaluation. The delay terms $[\tau_i, i = 1, 2, 3]$ account for differences in the lengths of the various

---

[*] A simple calculation from eq. 1 reveals the following relationship between the variance in τ and the variance of the measured phase: $\sigma_\tau \doteq \sigma_\theta(\sqrt{2})/[360(F_2 - F_1)]$. An uncertainty, $\sigma_\tau = 0.1$ ns, is commensurate with $\sigma_\theta = 0.01$ degree.

signal paths. The IF signal results from the argument differences of the input signals, which causes phase-noise cancellation to the following degree:

$$\theta_n(t + \tau_3) - \theta_n(t + \tau_1). \tag{6}$$

The variance* of this IF phase signal is equal to

$$\sigma^2_{\theta_n} = E[\theta_n(t + \tau_3) - \theta_n(t + \tau_1)]^2 = 2[R_{\theta_n}(0) - R_{\theta_n}(\tau)], \tag{7}$$

where $\tau = \tau_3 - \tau_1$. When $\tau = 0$, there is perfect cancellation. For a worst-case noise distribution,[†] assuming $\tau \leq 100$ ns, and an IF bandwidth ≤ 500 Hz the PM-S/N is improved in excess of 76 dB. Phase noise is similarly canceled in the phase-reference-path mixer.

The second phase-noise-cancellation mechanism arises from the use of a phase-reference signal. The difference in phase between the measurement signal and the phase-reference signal is detected. Phase noise common to both signals is rejected. This mechanism cancels phase noise originating in the source signal and the 0.495-GHz signals shown in Fig. 5. The cancellation exceeds 40 dB for the COTMS phase detector.

The combined effectiveness of the above mechanisms was measured by deliberately adding sinusoidal phase modulation exceeding 20 degrees peak to peak to the microwave source channel. No increase in the variance of a phase measurement (typically 0.01 degree) was detected.

4.5 Thermal stability

The rapid comparison technique of measurement described in Section 3.4 allows slowly varying changes in the test system lying external to the comparison switches to be canceled in the difference measurements. Changes in the transmission parameters of components lying inside the switches are not canceled. The latter component count is large due to the need to switch among the many test ports. The primary cause of parameter change is temperature fluctuation.

The temperature of the component assembly was stabilized in each test set by attaching it to a large aluminum plate, which in turn is surrounded by an insulating material. The composite structures have a thermal time constant exceeding 8 hours. This design has made thermal drift of these components a negligible source of error. The cables that connect the DUT to this circuitry are not enclosed in the stabilized environment and are a significant source of error (see Section 5.2).

---

* The stochastic variable θ_n is assumed to be a wide sense stationary process.[4]
† All energy concentrated at the extreme edges of the 500-Hz IF bandwidth.

4.6 Test port impedance invariance

By careful design, the impedance seen looking into the test ports used for simple insertion-loss measurements varies less than 2 percent from the nominal characteristic value of the coaxial line or waveguide. This is necessary to minimize reflection errors. With current hardware, it is not possible to achieve this impedance purity on the more complicated S-parameter switching networks. For measurements on these ports, the reflection errors are mathematically removed after the actual test set impedances are determined. This determination is accomplished through the measurement of calibration standards and a special hardware design.[3]

The S-parameter hardware shown in Fig. 4 is designed so that the impedances seen looking into each test port are constant, regardless of which parameter is measured. This invariance makes all S-parameter measurements referenced to the same impedances* and allows for the selfmeasurement of the physical impedances $Z1$ and $Z2$ seen by the DUT. This consistency allows the transformation of the measured data into an S-parameter representation free of reflection errors.

The invariance of the test port impedances in each test system is achieved by the use of isolators, attenuators, and the directivity of couplers to mask impedance changes caused by the switches. Variation of test port impedances of less than 0.05 percent has been achieved.

V. MEASUREMENT ERRORS

5.1 General

The nature of error mechanisms must be understood to be able to predict uncertainties that may arise under actual test conditions. This understanding was obtained during the development of the two test systems by directly characterizing the error-producing mechanisms and then by observing the errors in characterizing networks of predictable properties. Confidence was obtained from the consistency of the predicted errors and observed errors. The most important error-producing processes in the appliques are: thermal instabilities, nonlinearities, crosstalk, second-order-noise products, and impedance-reflection errors.

5.2 Thermal Instabilities

Thermal instabilities, which cause drift of the apparatus in the comparison unit between calibration and device measurements, are the

---

* In the $S11$ switch configuration, the detected loss and phase is directly related to $S11(Z1, Z2)$ of the device under test; $Z1$ and $Z2$ are the test port impedances. Once $Z1$, $Z2$ and the four-parameter set $S(Z1, Z2)$ are determined, it is possible through known transformations to obtain another representation such as $S(50, 50)$. The transformed parameters are then free of reflection errors.

largest source of uncertainty in absolute measurements. This error mechanism was anticipated in the system designs and measures were taken to stabilize the temperature of critical components. These measures are discussed in Section 4.5.

The paths that connect the test set connectors to the DUT are not controlled in temperature. These paths typically contain several feet of coaxial cable to achieve a flexible connection to the DUT. In the case of waveguide measurements, they also contain coax-waveguide transducers.* Careful measurements have correlated almost all of the observed output data drifts to temperature changes in these external connecting paths. The following sensitivities in both test sets have been observed:

$$\Delta\theta/\Delta T \doteq 0.1°/F° \text{ per GHz} \tag{8}$$

and

$$\Delta L/\Delta T \doteq 0.01 \text{ dB/F° per GHz.} \tag{9}$$

External path temperature cycling of 1°F peak to peak has been observed over a 1-hour period in the air-conditioned laboratory environment. The slowly varying thermal drifts do not cause significant uncertainties in the more critical differential measurements of delay [see eq. (1)] and loss slope.

5.3 System nonlinearities

The onset of nonlinearities in the test systems determines the high-signal-level limit of operation. Signal levels and components have been chosen to assure a measurement uncertainty less than 0.001 dB and 0.01 degree due to deviations from linear detection. Devices with gain are measured at a reduced excitation level so that the output-signal level lies in the linear-detection region.

One technique used to confirm linear performance consists of measuring a 6-dB loss unbalance between the two comparison-switch portions at the highest level and at a lower level. Adequate isolation exists between the comparison switch and the level-adjusting network to avoid errors due to impedance changes. The differences between the nominal 6-dB measurements are then used as a measure of errors caused by nonlinear behavior. The data indicates deviations from linear behavior are within accuracy objectives for both test sets. The components that limit linear behavior are the modulators in the heterodyne circuit.

---

* The coax-waveguide transducers are reciprocal and low loss for the four S-parameter measurements. The transducers include isolators and matching attenuators for the simple insertion-loss measurements.
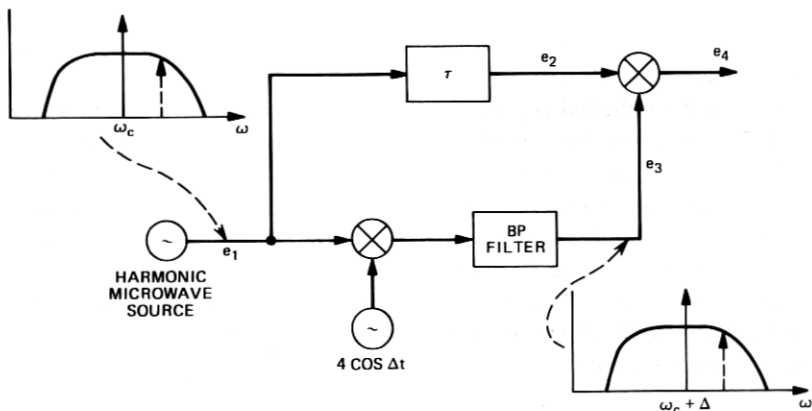
Fig. 6—Second-order noise product mechanism.

5.4 Crosstalk

Measurement uncertainties occur for DUTs with high loss when signals can reach the detector by other paths than through the DUT. By design, these leakage signals are more than 80 dB below the zero-loss-detected signal. For a DUT with loss Mx(dB), the uncertainty due to leakage or crosstalk is as follows:

$$|\text{Uncertainty (dB)}| < 8.68 \times 10^{Mx-80/20} \tag{10}$$

$$|\text{Uncertainty (deg)}| < 57.3 \times 10^{Mx-80/20}. \tag{11}$$

For example, the uncertainties for a device having 60 dB of loss could be 0.9 dB and 5.7 degrees. Crosstalk uncertainties are removed from reflection-coefficient and return-loss measurements but not from transmission measurements.* The second uncertainty term in eq. (3) accounts for this crosstalk.

5.5 Second-order noise products

The high degree of correlation between the RF signal and the RF local oscillator signal in both appliques leads to a small bias in the measured data. The mechanism can be understood by observing the simplified diagram of half of the comparison heterodyne section shown in Fig. 6. The harmonically generated microwave signal e_1 has associated with it a noise spectrum whose envelope is determined by the YIG filters and the spectral shape of the noise phenomena. The phase noise spectral shape typically follows a $1/\Delta f$ decay about the carrier frequency. The amplitude noise is typically flat and is significant only

---

* The removal of crosstalk uncertainties from the transmission measurement is possible with additional calibration measurements and data processing.

in the 4- to 12-GHz test set due to the use of TWT amplifiers with noise figures exceeding 40 dB.

A frequency-shifted replication of the noise spectrum of e_1 is present on the local oscillator signal e_3. A noise component on e_1, illustrated in Fig. 6 as a dashed line, interacts in the converter with a replica of the same component on e_3 to produce a coherent IF signal. The cumulative effect of all noise components produces a small signal at frequency $\Delta = 495$ MHz, leading to a bias in the measured quantities.

A detailed analysis[*] of the phenomena (see Appendix) indicates that the average value of the IF signal amplitude must be adjusted by the multiplicative factor,

$$[1 + Ram(\tau) + Rpm(\tau)]. \tag{12}$$

$Ram(\tau)$ and $Rpm(\tau)$ are the autocorrelation functions of the AM and PM noise spectrums, respectively, that are common to the signals e_1 and e_3. Similarly, the phase is adjusted by the additive factor,

$$[2\,Ram/pm(\tau)]\ \text{radians}. \tag{13}$$

$Ram/pm(\tau)$ is the cross-correlation function of the AM and PM noise spectrums. The parameter (τ) is the delay difference between the two paths to the converter shown in Fig. 4. It is therefore a function of the delay through the DUT.

The uncertainty caused by this second-order-noise interaction is proportional to the changes in the above terms due to the differential nature of the measurements [see eqs. (4) and (5)]. These uncertainties are to first order:

$$\text{Uncertainty (dB)} = 8.68[R\acute{a}m(\tau) + R\acute{p}m(\tau)](\tau x - \tau z) \tag{14}$$

$$\text{Uncertainty (deg)} = 115[R\acute{a}m/pm(\tau)](\tau x - \tau z). \tag{15}$$

The delay difference $(\tau x - \tau z)$ is the difference in delay between the DUT and the calibrating device. The prime denotes the first derivative with respect to (τ).

This analysis gave the qualitative understanding of this phenomena that led to the use of an intermediate stage of heterodyne conversion to reduce source noise (see Section 4.4). A quantitative understanding is prevented by a lack of knowledge of the noise-process statistics. Measurements made to reveal these uncertainties have shown that they are negligible for relatively broadband networks and for differential measurements such as delay and loss slope. Uncertainties of 0.01 dB and 0.03 degree were observed on the steep skirts of a 10-GHz

---

[*] Assuming the heterodyne converter is approximated as forming the product $e_2 \cdot e_3$.

cavity filter with a 40-MHz bandwidth. The uncertainties decrease directly with frequency since the phase noise dominates (see Section 4.4). These uncertainties are commensurate with the performance discussed in Section 2.3.

5.6 Errors from impedance mismatches

Errors are made in measuring a DUT when this device, calibration standards, and the test set terminals have impedances that differ from the assumed nominal values. In the microwave test systems, these errors are quite significant and are fundamentally different in the various measurement modes.

The simplest mode is the measurement of insertion transmission. The impedance mismatch uncertainty in measuring either the forward- or reverse-scattering parameters S_{21} and S_{12} has been discussed by many authors.[1,2,5] A general relationship is:

$$\frac{\overline{S_{ij}}}{M_{ij}} = \frac{1 - \rho_g \overline{S_{jj}} - \rho_l \overline{S_{ii}} + \rho_g \rho_l \overline{\Delta S}}{1 - \rho_g \rho_l}, \tag{16}$$

where

M_{ij} is the voltage-scattering parameter actually measured between the test set generator impedance Zg and the test set load impedance Zl.

$$\rho_g = \frac{Zg - Rg}{Zg + Rg} \qquad \rho_l = \frac{Zl - Rl}{Zl + Rl}. \tag{17}$$

The S-parameters are those that would be obtained if the test set had ideal impedances Rg and Rl.

In both microwave test systems, the insertion transmission measurements are made with relatively simple hardware. This simplicity allowed the impedances of the test ports to be kept within 2 percent of nominal. Examples of the impedance mismatch uncertainty that can occur in measuring unknowns (assuming $|\overline{S_{12}} \cdot \overline{S_{21}}| \leqq 1$; $|\rho_g| \leqq 0.01$, $|\rho_l| \leqq 0.01$) of varying input and output return losses have been computed from eq. (16) and are given below:

DUT Return Loss*	Max. Amplitude Error	Max. Phase Error
40	0.0035 dB	0.023°
30	0.0072 dB	0.048°
20	0.0191 dB	0.126°

The impedance or reflection coefficient of a DUT is determined from one measurement of the DUT and one measurement on each

---

* Return loss $= -20 \log |\overline{S_{ii}}| \quad i = 1, 2.$

of three calibration standards. The standards are typically two reactive circuits (nominally an open and a short) and a resistive circuit (Zs) nominally matched to a transmission line characteristic impedance (Rs). The uncertainty that is incurred if $Zs \neq Rs$ is (Ref. 2):

$$M - \Gamma = \frac{\Gamma - \rho_s}{1 - \rho_s \Gamma} - \Gamma \doteq \rho_s(\Gamma^2 - 1) \tag{18}$$

$$\rho_s = \frac{Zs - Rs}{Zs + Rs}. \tag{19}$$

M is the measured voltage-reflection coefficient and Γ is the reflection coefficient that would be measured if $Zs = Rs$. ρ_s is smaller than 0.001 for the better resistive standards. The errors arising from uncertainties in the reactive standards are much smaller and are ignored. Notice that (18) vanishes for $\Gamma = \pm 1$. This occurs when the reflection measurement reduces to a differential comparison of the DUT with either the open or short standard. Notice that the use of calibration standards makes the mismatch errors dependent on the quality of the calibration standards and not upon the impedances of the test system's terminals.

Four-parameter characterizations are made with complex switching hardware in which the test-port impedances can vary with frequency up to 20 percent from the design values. The large impedance-mismatch uncertainties that could arise are reduced by processing measurements of the DUT with measurements on calibration standards. The characterizations are performed in three steps. First, all S parameters defined with respect to the actual test set impedances, $Z1$ on port 1 and $Z2$ on port 2, are determined (see Section 4.6). These parameters are, by definition, free of impedance-reflection errors. Next, the impedances $Z1$ and $Z2$ are measured using the same three reflection coefficient standards mentioned above. Finally, these $S(Z1, Z2)$ parameters are transformed to another representation, most commonly $S(Rs, Rs)$. The reflection errors that arise in the transformed representation are dependent upon the accuracy to which $Z1$ and $Z2$ or their voltage-reflection coefficients ρ_1 and ρ_2 are characterized. Thus, the impedance mismatch errors are related to uncertainties in the calibration standards and not the test set impedances.

The quantities ρ_1 and ρ_2 are,[*] from eq. (18), approximately equal to ρ_{s1} and ρ_{s2}, respectively. ρ_{s1} and ρ_{s2} are the reflection coefficients of the resistive calibration standards R_{s1} and R_{s2} used on ports 1 and 2, respectively. The relationships between the measured parameters

---

[*] $|\rho_i| \ll 1 \quad i = 1, 2.$

$[S(Z_{s1}, Z_{s2})]$ and the error-free parameters $[S(R_{s1}, R_{s2})]$ are found by known transformations.[2]

$$\frac{S_{ij}(R_{s1}, R_{s2})}{S_{ij}(Z_{s1}, Z_{s2})} = \frac{1 - \rho_{si}S_{ii} - \rho_{sj}S_{jj} + \rho_{si}\rho_{sj}\Delta S}{(1 + \rho_{si})(1 - \rho_{sj})}\bigg|_{R_{s1}, R_{s2}}$$
$$\doteq 1 - \rho_{si}[S_{ii}(R_{s1}, R_{s2}) + 1]$$
$$- \rho_{sj}[S_{jj}(R_{s1}, R_{s2}) - 1]. \quad (20)$$

$$S_{ii}(Z_{s1}, Z_{s2}) = \frac{S_{ii} - \rho_{si} + \rho_{si}\rho_{sj}S_{jj} - \rho_{sj}\Delta S}{1 - \rho_{si}S_{ii} - \rho_{sj}S_{jj} + \rho_{si}\rho_{sj}\Delta S}\bigg|_{R_{s1}, R_{s2}}$$
$$\doteq S_{ii}(R_{s1}, R_{s2}) - \rho_{si}[1 - S_{ii}^2(R_{s1}, R_{s2})]$$
$$+ \rho_{sj}S_{ij}(R_{s1}, R_{s2})S_{ji}(R_{s1}, R_{s2}). \quad (21)$$

These relationships coupled with extensive experimental data were used to derive the uncertainty bounds given by eqs. (2) and (3).

VI. MEASUREMENT RESULTS

6.1 General

Ideally, measurement accuracy should be confirmed with network standards selected to accentuate various error mechanisms. At microwave frequencies, no complete set of such networks exists. The measurement results given below* examine accuracy with a few network standards whose properties are based upon geometric dimensions. Additional indications of accuracy are obtained from characterizations of a given network under different measurement conditions that are expected to give the same results, and by comparing characterizations on both test systems in the 3.7- to 4.2-GHz band of overlap.

6.2 Transmission measurements

6.2.1 Delay of an airline

The ability to accurately measure envelope delay is of critical importance to the development of transmission networks. The delay-measuring uncertainties in both measuring sets were evaluated by measuring an airline of known electrical length, one of the few available standards of delay. The data shown in Fig. 7 is a measurement of the delay of a 7-mm airline of 20.35 cm in electrical length. A frequency difference of 20 MHz was used in the on-line calculation of delay using eq. (1). The results show a measurement uncertainty of less than ±0.022 ns about the nominal delay of 0.678 ns.

---

* Errors caused by the failure of connectors to make good contact are not discussed. These errors are not significant for waveguide connections. For this reason, many of the networks measured for accuracy verification have waveguide connectors.
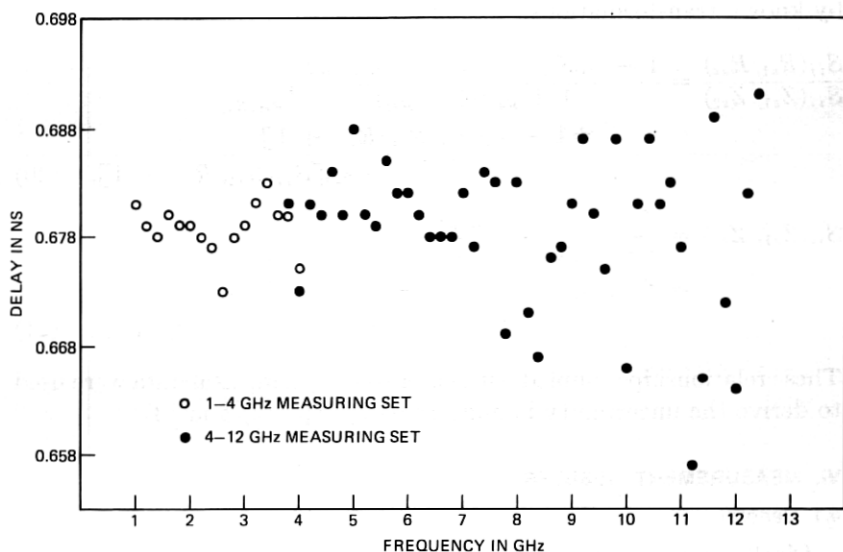
Fig. 7—Delay of an airline with a 20.35-cm electrical length.

6.2.2 Insertion parameters of a waveguide filter

The loss and delay of a narrow-bandwidth waveguide filter was measured on both test sets to compare their accuracy. Waveguide isolators were used to improve the impedances of the coax-waveguide transducers needed to make measurements on the 1- to 4-GHz test set. The same isolators were used in the measurement made on the 4- to 12-GHz test set so that the DUT would see essentially the same test set impedances in each measurement. The filter characteristic showing the passband and a portion of the stop band measured on the 1- to 4-GHz test set is shown in Fig. 8. Equivalent data taken on the 4- to 12-GHz test set (not shown) coincides point for point except at loss levels above 80 dB. At loss values above 80 dB, the measured loss is limited by crosstalk to about 88 dB.

The difference between characterizations on the two sets in a magnified portion of the passband is shown in Fig. 9. The worst-case loss and delay* differences are 0.004 dB and 0.08 ns. The average absolute differences are 0.0012 dB and 0.019 ns. These differences are less than the bound on the typical uncertainty computed from eq. (3), 0.005 dB and 0.1 ns.

---

* Delay was computed on-line using eq. (1) with a frequency difference of 1 MHz.
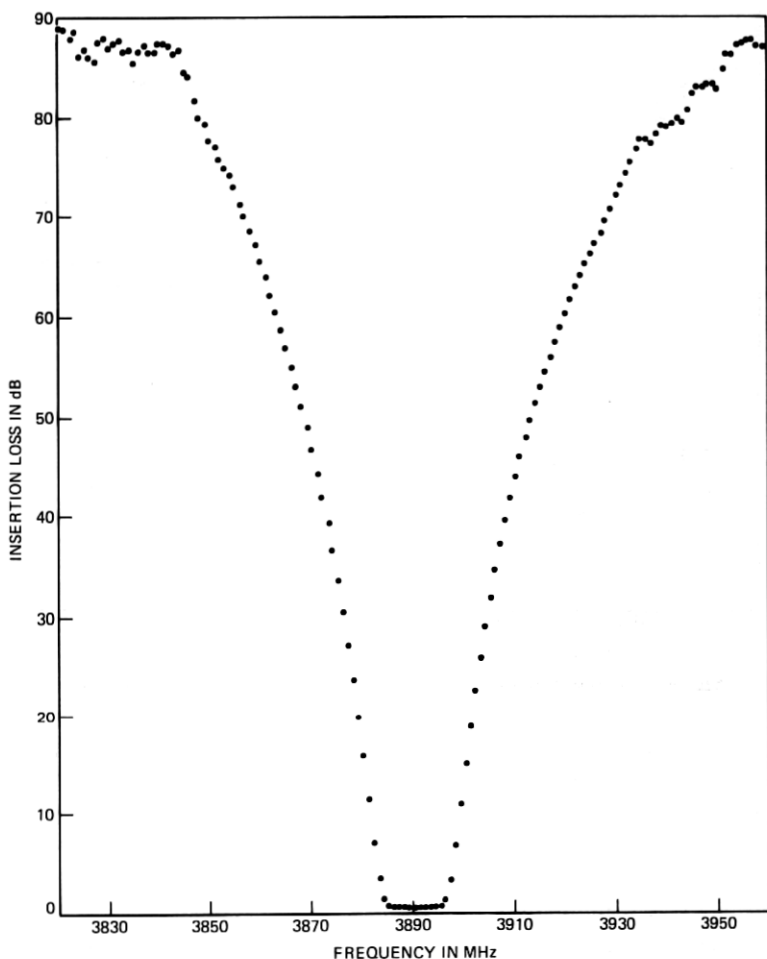
Fig. 8—Insertion loss of a waveguide filter measured on the 1- to 4-GHz measuring set.

6.2.3 Measurement stability

The insertion loss and phase of a 12-dB attenuator was measured at the beginning and end of a 20-minute time interval to evaluate the stability of insertion measurements. The attenuator was surrounded by thick insulation to increase its response time to temperature changes. Such precautions are sometimes necessary to make precise measurements at microwave frequencies depending on the temperature dependence of the DUT.
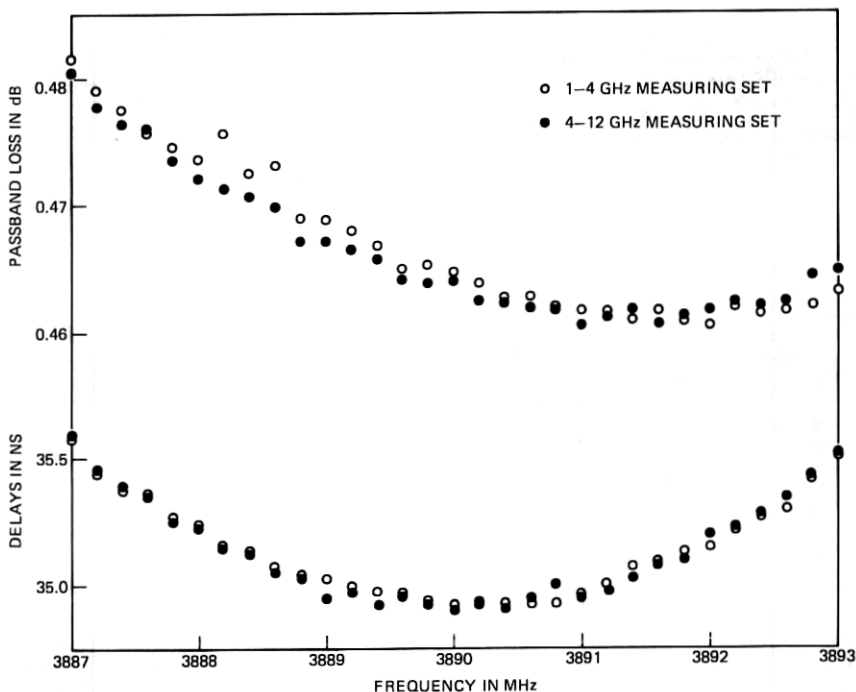
Fig. 9—Passband loss and delay of waveguide filter measurements.

The differences in the two measurements are shown in Fig. 10. The loss differences are typically smaller than 0.004 dB. The phase differences are approximately proportional to frequency as if there were a change in the electrical length of the attenuator or test-system circuitry. The data indicate an equivalent change in electrical length of less than 0.001 inch over the 20-minute interval. This corresponds to a change of less than four parts in one million in the more than 20 feet of equivalent circuit length associated with either measuring system (see Section 4.5).

6.3 Return-loss measurements

Return-loss or one-port characterizations are measured on the 4- to 12-GHz test set on both waveguide and coaxial test ports. These measurements are made on the 1- to 4-GHz test set using coaxial test ports. Low-loss transducers can be used on either set to make measurements in other connectors. The measurement of the DUT and calibration is under computer direction. Three calibration standards described by a constant magnitude and a phase that varies linearly with propagation coefficient are used. This description allows for the

correction of some perturbations from nominal values and for the mathematical translation of the reference plane of measurement. The calibration standards typically chosen are a nominal short circuit, open circuit, and a resistive termination. These features will be demonstrated below in the measurement of some precisely machined waveguide networks.

6.3.1 Inductive iris

A symmetric inductive iris 1.7 inches wide by 0.2 inch thick was constructed in WR229 waveguide and measured on both test systems. Measurements on the 4- to 12-GHz system were made with connection to a high-directivity magic-tee hybrid. Measurements on the 1- to 4-GHz system were made with connection to the internal coaxial hybrid through a lossless waveguide to coax transducer. Calibration was performed with three waveguide standards, a short, an offset short, and a match. A different set of standards was used on each test system. Figure 11 gives the measurement results on the 1- to 4-GHz system. Data obtained from the 4- to 12-GHz system (not shown) exhibit a mean absolute difference of 0.01 dB and 0.08 degree from
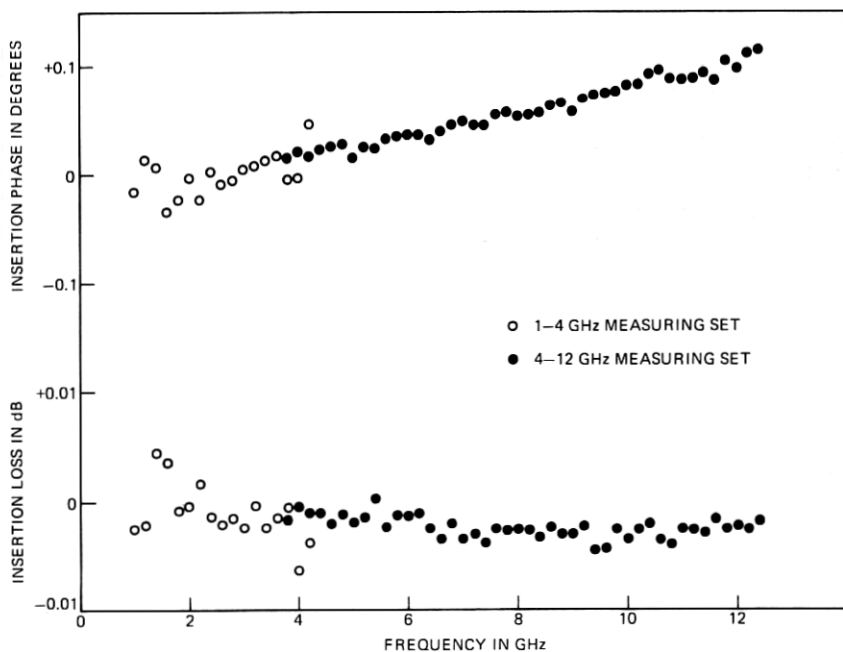

Fig. 10—Change in insertion loss and phase of a 12-dB attenuator after a 20-minute time interval.
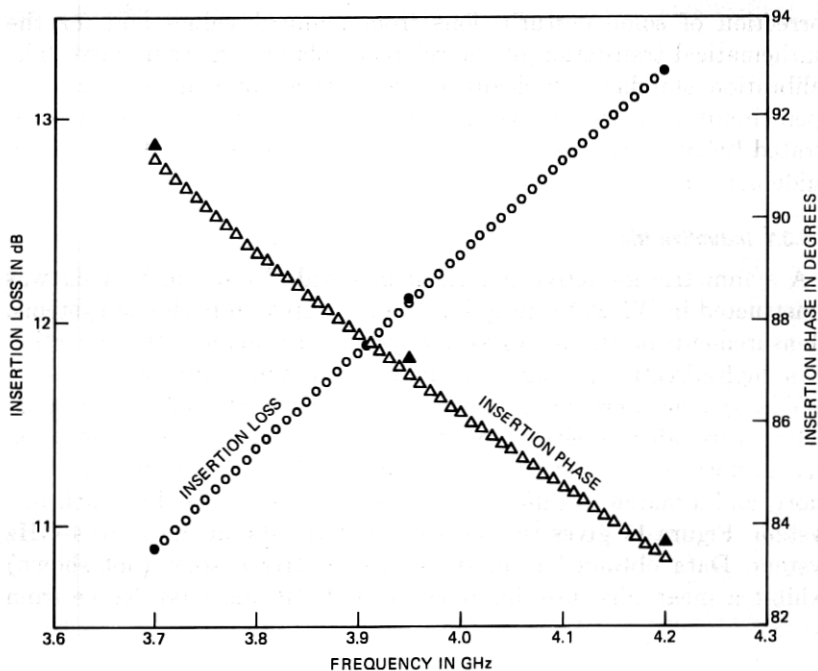
Fig. 11—Insertion loss and phase of a symmetrical inductive window 1.700 inches wide by 0.2 inch thick.

the 1- to 4-GHz system data, with peak differences of 0.03 dB and 0.15 degree. The solid data points are derived from theoretical computer computations based upon the mode-matching technique.[6] These differences are less than the uncertainty of 0.037 dB and 0.24 degree computed from eq. (2). Experimental results in the next section reveal that a major contributor to the uncertainties in these measurements is the deviations of the match from a zero reflection coefficient.

6.3.2 Offset short

A short circuit displaced 0.4090 cm in WR90 waveguide was measured as a circuit standard. This circuit has a reflection coefficient of unit magnitude (0 dB) and an angle of −90 degrees in the middle of the 10.7- to 11.7-GHz microwave radio band. The calibration standards used for the measurement were a zero length short, a match, and a short offset by 0.8197 cm. The latter calibration standard has a reflection coefficient of unit magnitude and an angle of 180 degrees in midband. The match has a return loss exceeding 60 dB. The measurement of this circuit should produce the worst-case uncertainties since
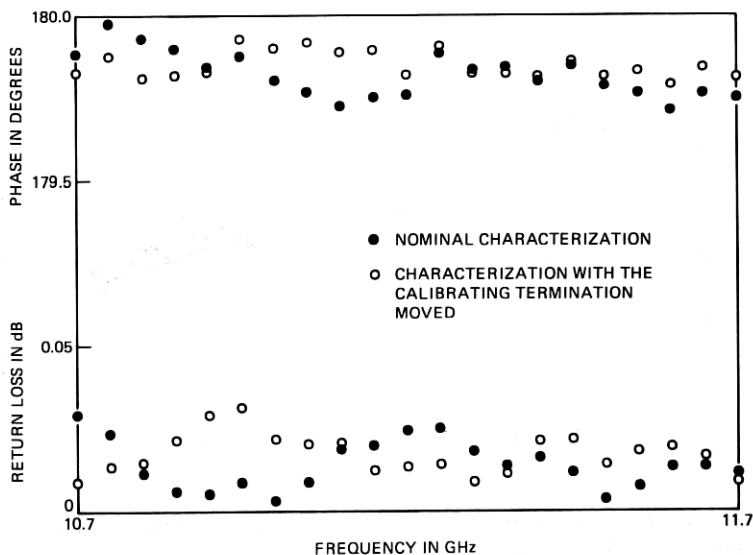
Fig. 12—Return loss of an offset short in WR90 waveguide.

its reflection coefficient has the greatest distance on the Smith chart from the reflection coefficients of the calibrating standards.

The measurement results are shown in Fig. 12. The measurement reference plane was mathematically moved to the plane of the circuit's short circuit by an on-line program. The nominal characterization at this displaced plane is a reflection coefficient of unit magnitude and constant 180-degree phase angle. Two characterizations are presented, one with the tapered absorber in the match in its nominal position and a second with the absorber moved 0.83 cm ($\sim\lambda/4$) within its electroformed waveguide. The changes in the characterizations reveal that deviations of match from a zero reflection coefficient are a significant source of measurement uncertainty. The worst-case deviations are less than the uncertainties of 0.052 dB and 0.34 degree computed from eq. (2).

6.4 Four-parameter characterizations

Four-parameter or two-port characterizations are measured on both microwave test sets using automatically switched hardware and a computer-directed calibration technique. These features were briefly discussed in Sections 2.2 and 5.6. Voltage-scattering parameters (S parameters) are computed in real time. The calibration-standard models used assume a constant magnitude and a phase that varies linearly with propagation coefficient. This description allows for the
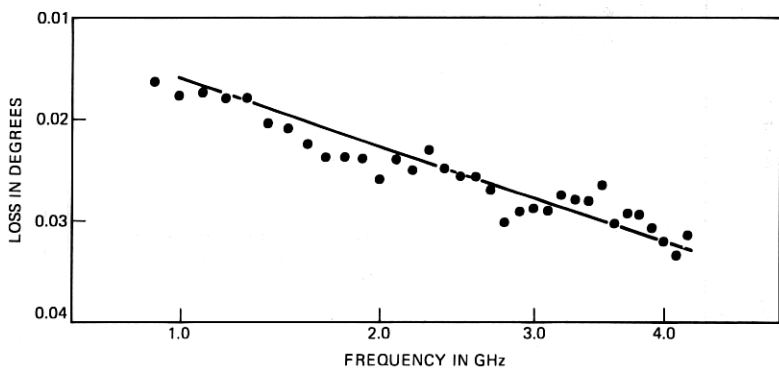
Fig. 13—*S*21 phase of a 50-ohm airline.

correction of some perturbations from nominal values and for the translation of the reference planes of measurement. Some of these features will be demonstrated in the measurements below. Parameter representations other than *S* parameters are available through processing following the measurements.

6.4.1 Airline characterizations

An airline is a two-port network whose characteristics are precisely known. Errors can arise in characterizing an airline if the test set impedances deviate significantly from nominal. Impedance deviations
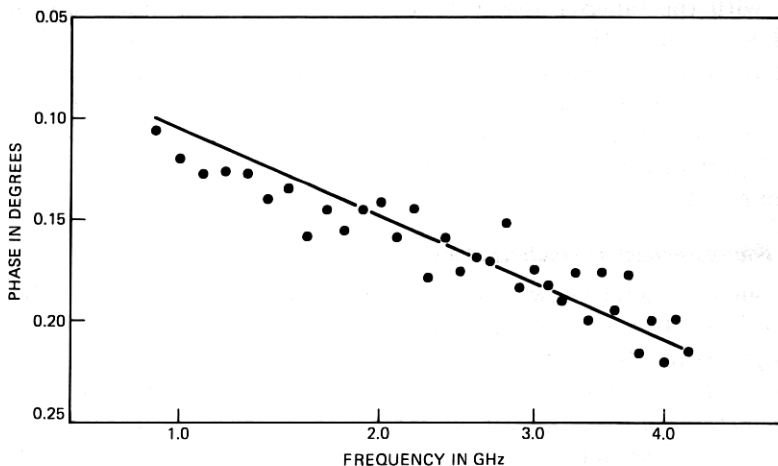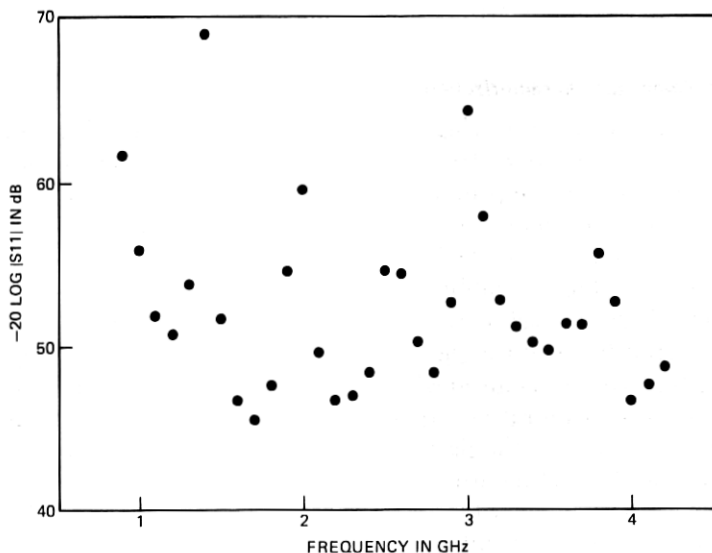

Fig. 14—*S*21 magnitude of a 50-ohm airline.

Fig. 15—*S*11 magnitude of a 50-ohm airline.

in excess of 20 percent are observed in the test sets. These errors are avoided by the calibration method discussed in Section 5.6.

A 30-cm-long 14-mm airline was characterized on the 1- to 4-GHz measuring system to illustrate these points and to demonstrate the accuracy obtained. The *S*21 measurements are plotted in Figs. 13 and 14 on a square-root-of-frequency scale. The reference planes of measurement were translated to the center of the airline so that the phase data is the difference between the measured airline and an ideal airline. Observe that the data indicates characteristics nearly linear* with respect to the square root of frequency as expected from theoretical models, taking skin losses into account.[2] The maximum deviation from linear is 0.004 dB and 0.05 degree. The typical deviation derived from eq. (3) is predicted to be less than 0.005 dB and 0.04 degree. An *S*21 measurement was also made without calibration to demonstrate the accuracy improvement provided by computationally removing the test set impedance-reflection errors. Deviations from a square-root-of-frequency characteristic in excess of 0.1 dB and 0.7 degree were observed.

The magnitude of *S*11 (dB) is shown in Fig. 15. The uncertainty of this measurement is dominated by deviation of the resistive calibration

---

* The solid line in Fig. 14 was extrapolated from resonant *Q* measurements made at 250 MHz.

standard from 50 ohms, corresponding to a reflection coefficient uncertainty of 0.005 (46 dB).

6.4.2 Transistor characterization

The 1- to 4-GHz measuring system is frequently used for the characterization of microwave transistors to be used in amplifier circuits. Their small size and impedances that vary considerably from 50 ohms make them particularly difficult to characterize accurately. Two characterization techniques have been used. The first technique uses simplified handling by calibrating with large coaxial standards at the interface of the transistor jig and test set. The defined reference planes are then translated to the jig-transistor interface making the approximation that the jig is an ideal 50-ohm transmission line. The second technique uses calibration standards of the same size scale as the transistor inserted at the jig-transistor interface. The parasitic circuit elements of these standards are significantly smaller than those associated with the transistor jig. A detailed characterization effort is under way so that a definitive accuracy evaluation can be made.

Measurements of $S11$ using the two techniques to characterize a beam-leaded transistor mounted on a 0.1-inch-square substrate are
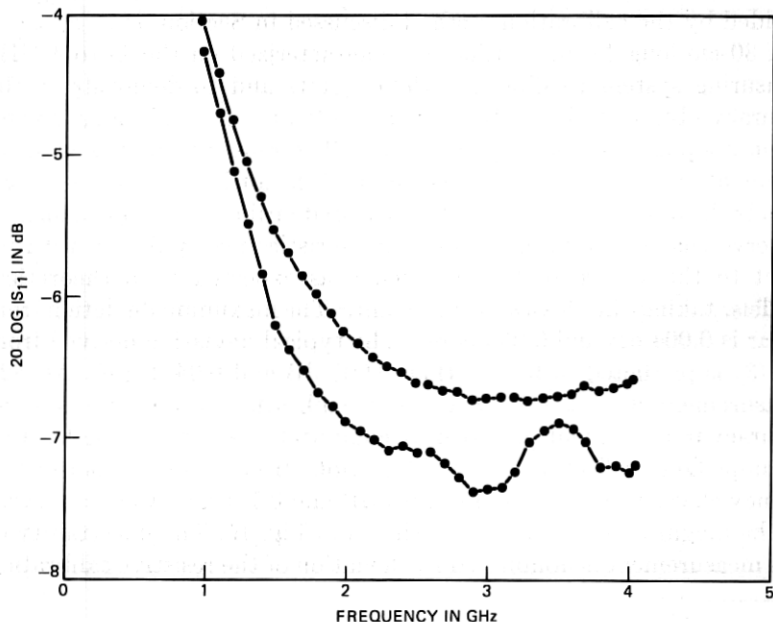

Fig. 16—Input reflection coefficient of a beam-leaded microwave transistor.
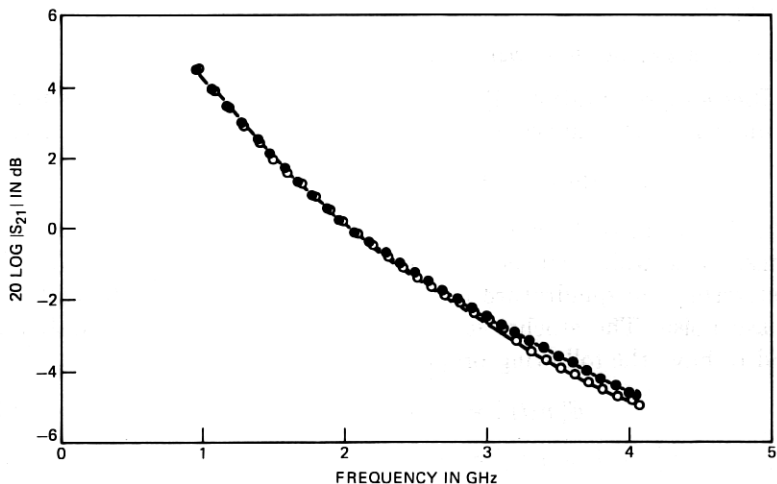
Fig. 17—Forward scattering parameter of a beam-leaded microwave transistor.

shown in Fig. 16. The top curve is the characterization using the transistor-sized standards. This curve is free of the impedance cycling with frequency that is evident in the second curve measured with the coaxial standards. This cycling cannot be attributed to the transistor and is found in measurements on the jig with the transistor replaced with a through connection.

The measurements of $S21$ using the two calibration techniques is shown in Fig. 17. The measurements using the coaxial standards cycle about the measurements using the transistor-sized standards, ending up 0.5 dB lower at 4 GHz. These results reveal that measurement accuracy can be improved by calibration directly at the interface of the DUT and the test set.

VII. SUMMARY

The development of two general-purpose network analyzers covering the frequency range of 0.9 to 12.4 GHz has been discussed. These network analyzers were developed to provide flexible, fast, and accurate circuit characterizations, which are necessary feedback in the circuit design process.

Automatic control and highly accurate baseband detection is provided by the Computer Operated Transmission Measuring Set. The techniques used to extend baseband-measurement capabilities to microwave frequencies while retaining accuracy were discussed. The most prominent sources of measurement errors were quantitatively examined. Measurements results that confirm accuracy were presented.

APPENDIX

Analysis of Second Order Noise Products

Rice's representation (Ref. 4, p. 374) of a stochastic process is convenient for the analysis of the heterodyne process modeled by Fig. 6.

$$e_1 = \sin(\omega_c t) + n(t)\sin(\omega_c t) + m(t)\cos(\omega_c t). \tag{22}$$

The first term is the normalized carrier signal. The second term is in phase noise which can be thought of as AM noise for small $n(t)$. The last term is in quadrature noise which can similarly be thought of as phase noise. The stochastic variables are assumed to be stationary and to have the following properties.*

$$E[n(t)] = E[m(t)] = 0. \tag{23}$$

$$E[n(t+\tau)n(t)] = Ram(\tau) = Ram(-\tau). \tag{24}$$

$$E[m(t+\tau)m(t)] = Rpm(\tau) = Rpm(-\tau). \tag{25}$$

$$E[m(t+\tau)n(t)] = Ram/pm(\tau) = -Ram/pm(-\tau). \tag{26}$$

The delayed signal e_2 and the up-converted signal e_3 are given by

$$e_2 = \sin(\omega_c t + \omega_c \tau) + n(t+\tau)\sin(\omega_c t + \omega_c \tau)$$
$$+ m(t+\tau)\cos(\omega_c t + \omega_c \tau). \tag{27}$$

$$e_3 = 2\sin(\omega_c + \Delta)t + 2n(t)\sin(\omega_c + \Delta)t$$
$$+ 2m(t)\cos(\omega_c + \Delta)t. \tag{28}$$

The output converter is approximated as forming the product $e_4 = e_2 \cdot e_3$.

$$e_4 = \cos(\Delta t - \omega_c \tau)$$
$$+ [n(t+\tau)n(t) + m(t+\tau)m(t)]\cos(\Delta t - \omega_c \tau)$$
$$+ [m(t+\tau)n(t) - n(t+\tau)m(t)]\sin(\Delta t - \omega_c \tau)$$
$$+ [n(t+\tau) + n(t)]\cos(\Delta t - \omega_c \tau)$$
$$+ [m(t+\tau) - m(t)]\sin(\Delta t - \omega_c \tau). \tag{29}$$

Filterable tones falling at $2\omega_c$ have been omitted from eq. (29).

Taking the expected value of e_4 and substituting the properties of eqs. (23) through (26) yields,

$$E(e_4) = \cos(\Delta t - \omega_c \tau) + [Ram(\tau) + Rpm(\tau)]\cos(\Delta t - \omega_c \tau)$$
$$+ 2Ram/pm(\tau)\sin(\Delta t - \omega_c \tau). \tag{30}$$

$$E(e_4) \doteq [1 + Ram(\tau) + Rpm(\tau)]\cos[\Delta t - \omega_c \tau - 2Ram/pm(\tau)]. \tag{31}$$

---

* $E[\cdot]$ denotes expected value. If $Ram(\tau) = Rpm(\tau)$, then the noise process also models an additive as well as a modulating stationary process.[4]

The amplitude and phase of the mean IF signal e_4 are seen in eq. (31) to be modified by the noise present on the microwave signals.

REFERENCES

1. W. J. Geldart, G. D. Haynie, and R. G. Schleich, "A 50 Hz-250 MHz Computer-Operated Transmission Measuring Set," B.S.T.J., *48*, No. 5 (May 1969), pp. 1339–1381.
2. J. G. Evans, "Measuring Frequency Characteristics of Linear Two-Port Networks Automatically," B.S.T.J., *48*, No. 5 (May 1969), pp. 1313–1338.
3. J. G. Evans, "Linear Two-Port Characterization Independent of Measuring Set Impedance Imperfections," Proc. IEEE, *59*, No. 4 (April 1968), pp. 754–755.
4. A. Papoulis, *Probability, Random Variables, and Stochastic Processes,* New York: McGraw-Hill Book Company, 1965, pp. 300–340.
5. D. Leed, "An Insertion Loss, Phase and Delay Measuring Set for Characterizing Transistors and Two-Port Networks Between 0.25 and 4.2 gc," B.S.T.J., *45*, No. 3 (March 1966), pp. 397–440.
6. N. Marcuvitz, *Waveguide Handbook,* New York: McGraw-Hill, 1951, pp. 255–257.